CHEMIJA. 2019. Vol. 30. No. 3. P. 136–145

Investigation of sodium borohydride and hydrazine oxidation on gold nanoparticles modified zinc–cobalt coating

Aušrinė Zabielaitė*,

Aldona Balčiūnaitė,

Dijana Šimkūnaitė,

Jūratė Vaičiūnienė,

Algirdas Selskis,

Leonas Naruškevičius,

Loreta Tamašauskaitė-Tamašiūnaitė,

Eugenijus Norkus

Department of Catalysis,
Center for Physical Sciences and Technology,
3 Saulėtekio Avenue,
10257 Vilnius, Lithuania

This work presents the investigation of the electrochemical oxidation of hydrazine and sodium borohydride ions in alkaline solutions on the Au nanoparticles modified ZnCo coating surface, which was deposited on the titanium substrate (termed as AuZnCo/Ti). The AuZnCo/Ti catalysts were prepared via a facile electrochemical deposition technique followed by a simple and low-cost galvanic displacement. Scanning electron microscopy, energy dispersive X-ray analysis and inductively coupled plasma optical emission spectroscopy were used for characterization of the prepared catalysts surface morphology, structure and composition, whereas their electrocatalytic behaviour was investigated for the electrochemical oxidation of hydrazine and sodium borohydride in an alkaline medium using cyclic voltammetry. It has been determined that the AuZnCo/Ti catalysts with Au loadings of 31, 63 and 306 μg cm^{-2} show enhanced catalytic activity towards the electrochemical oxidation of both hydrazine and sodium borohydride as compared to that of the ZnCo/Ti catalyst.

Keywords: Au, ZnCo, hydrazine, borohydride, oxidation

INTRODUCTION

Among various renewable energy sources fuel cells (FC) are those that are progressively entering the market due to their intrinsic high efficiency, virtually pollutant-free and quiet operation, ultra-clean energy, fuel flexibility, reliability and scalability to a wide range of applications. Now FC research is focused on the realization of its potentials in portable and mobile electronic devices, such as mobile phones, mp3 players, notebooks, etc. [1–4]. Usually, such FCs are powered by liquid fuels, like alcohols, ethers, organic acids or inorganic compounds [5]. The possibility of selection of an appropriate fuel in relevance to the necessary operation conditions and specific requirements makes them extremely attractive in energy conversion systems. The intrinsic thermodynamic properties of some fuels containing a different kind of electrolyte, which can be used as a fuel in FCs, are described in Refs. [6, 7]. The superiority of direct borohydride and hydrazine fuel cells (DBFCs and DHFCs) that generate cell voltages of 1.64 and 1.61 V, respectively, was shown. The mentioned values substantially outperform those of ethanol (1.15 V), methanol (1.21 V), hydrogen (1.23 V), and formic acid (1.40 V) fuel cells. Direct borohydride and hydrazine fuel cells generate oxidation products that are environment-friendly and soluble in water. Borates (Eq. 1) or only nitrogen and water (Eq. 2) are formed by the following reactions [2, 7]:

* Corresponding author. Email: ausrine.zabielaite @ftmc.lt

$$BH^-_4 + 8OH^- \rightarrow BO^-_2 + 6H_2O + 8e^-$$

$$(E^0 = -1.24 \text{ V vs SHE}), \quad (1)$$

$$N_2H_4 + 4OH^- \rightarrow N_2 + 4H_2O + 4\,e^-$$

$$(E^0 = -1.16 \text{ V vs SHE}). \quad (2)$$

For those reasons, the aforementioned fuels are rather promising since (contrary to the other fuels) they have no carbon atoms in their molecules to produce carbon monoxide or dioxide. Therefore, no exhaust of greenhouse gases is observed. Moreover, the absence of any carbon species poses no risk to poison the electrocatalysts that are employed in FCs [5, 7]. Yet more, sodium borohydride and hydrazine have a rather high hydrogen content of 10.8 wt.% and 12.5 wt.%, respectively, and can be used for hydrogen production. All of them are prone to spontaneous hydrolysis by the reactions [2, 5, 7–10]

$$NaBH_4 + H_2O \rightarrow NaBO_2 + 4H_2, \quad (3)$$

$$N_2H_4 + H_2O \rightarrow N_2H^+_5 + OH^-. \quad (4)$$

Nevertheless, borohydride hydrolysis as hydrogen generation process occurs on the ground of the reaction (3), however, in the case of hydrazine, hydrogen production is known to proceed via decomposition of the latter by two routes with the formation of different products as noted below [11]:

$$N_2H_4 \rightarrow N_2 + 2H_2, \quad (5)$$

$$3N_2H_4 \rightarrow N_2 + 4NH_3. \quad (6)$$

Reaction (6) is an adverse one and leads to an undesirable release of the NH_3 by-product that reduces the amount of hydrogen generated. Furthermore, even small amount of ammonia causes deactivation of the catalyst and is a poison for fuel cells [12].

On the other hand, the aforementioned hydrolysis reactions (Eqs. 3 and 4) and chemical decomposition of hydrazine (Eqs. 5 and 6) are considered as strongly unfavoured ones in DBFCs and DHFCs operation, since they lead to incomplete fuel oxidation, furthermore, decrease the faradaic efficiency and reduce the power density of FC. Despite the dual relevance of hydrazine and sodium borohydride to act as a hydrogen source or as an anodic fuel for DHFCs and DBFCs, the need for the proper catalyst emerges. The most commonly used catalysts in direct fuel cells are still the noble ones. Commercial employment of those catalysts is hindered by the high costs of the main constitutive material of the electrode. This problem is handled by using single-, double- and multiple-component catalysts containing non-precious transition metals such as Ni, Co, Fe, Zn, et al. Such an approach allows reducing the amount of the expensive material used and the price of the catalyst simultaneously. Decoration of transition metals by small amounts of the noble metal is also advantageous, since it satisfies cost-efficient requirements for the catalyst, on the one hand, and the pursuit of essential complete oxidation, on the other. The complete oxidation for hydrazine and borohydride has been observed at noble metal catalysts, such as Au and Pt-group metals [13–16]. Moreover, recent electrochemical studies suggest that the Pt- or Au-based binary electrocatalysts denoted as PtM or AuM (M = Co, Ni, Cu, Fe, Zn) for both DBFC [17–28] and DHFC [29–35] not only permit to control the content of the catalyst, but they definitely perform the apparently improved activity and stability as compared to monometallic ones.

Nowadays, non-precious systems for DBFC, such as Ni–Cr, [36], Ni/ZnNi/Ni/Cu [37] and CoNiMnB [38] are of particular interest; however, they have not been adequately studied yet. The simple galvanic replacement of Zn by Pd or Au in the Ni–Zn coating enabled fabrication of the stable nanostructures of ternary or even quaternary catalysts like Ni/PdNi [39] or Cu/Ni/AuNi [40] with a reduced content of noble metal that seem to be promising ones for the direct borohydride fuel cells. A set of works based on non-precious Co-containing [41–49], Ni, Ni binary and ternary alloy electrocatalysts [41, 42, 45, 49–53] for DHFCS have emerged either. Asazawa and co-workers presented a single-phase disordered noble metal-free $Ni_{60}Co_{40}$ alloy electrocatalyst with a 6-fold increase in catalytic hydrazine hydrate oxidation activity over today's benchmark catalyst [46]. However, the chemical decomposition of hydrazine was shown to proceed simultaneously over a broad range of potentials and yet more the rate of this reaction was found to be enhanced by the presence of the faradaic current. This parasitic fuel loss has serious implications for the operation efficiency of

hydrazine fuel cells in practice. On the other hand, the high electrochemical activity and stability for Ni and Co used as the anodes in DHFCS have been noted in Ref. [41]. However, their feasibility and promise for future fuel cell vehicles is restricted by the operating conditions, such as a large hydrazine concentration or relatively high temperature used. Therefore, the development of perfect electrocatalysts with outperforming characteristics at ambient conditions for DHFCS is industrially vital.

Based on a strong demand for an efficient and relatively inexpensive catalyst, here we present a simple approach for fabrication of the multiple-component catalyst system containing non-precious transition metals, such as ZnCo coating and a negligible amount of Au nanoparticles with the aim to use it as the anode in direct borohydride and hydrazine fuel cells. The ZnCo coating was electroplated on the titanium surface (denoted as ZnCo/Ti) and followed by its modification with Au nanoparticles using the galvanic displacement technique [19, 24, 27, 28, 30, 54]. This electrode is termed as AuZnCo/Ti. The electrocatalytic activity of the prepared catalysts was investigated towards the hydrazine oxidation reaction (HOR) and borohydride oxidation reaction (BOR) in an alkaline medium using cyclic voltammetry. Scanning electron microscopy (SEM), energy dispersive X-ray analysis (EDX) and inductively coupled plasma optical emission spectroscopy (ICP-OES) were used for the characterization of the morphology, structure and composition of the prepared catalysts.

EXPERIMENTAL

Chemicals

Titanium foil (99.7% purity, 0.127 mm thick), N_2H_4, $NaBH_4$, $HAuCl_4$, $CoSO_4$ and ZnO were purchased from Sigma-Aldrich Supply. H_2SO_4 (96%) and NaOH (99%) were purchased from Chempur Company. All chemicals were of analytical grade. Deionized water with the resistivity of 18.2 MΩ cm^{-1} was used to prepare all the solutions.

Fabrication of catalysts

Prior to ZnCo coating deposition, the titanium plates (1 × 1 cm) were pre-treated with SiC emery paper (grade 2500) and MgO powder, degreased with acetone, then etched in diluted H_2SO_4 (1:1 vol) at 90°C temperature for 10 s and finally rinsed with deionized water. Then, the ZnCo coatings with a thickness of ~5 μm were deposited on the Ti surface via electrodeposition from the electrolyte containing 20 g l^{-1} $CoSO_4$, 100 g l^{-1} NaOH, 40 g l^{-1} N-(2-Hydroxyethyl) ethylenediamine, 10 g l^{-1} ZnO (denoted as the ZnCo plating bath) [54–56]. The plating bath operated at 20 ± 2°C temperature. Stainless steel sheets were used as the anodes and the Ti sheet was used as the cathode. The deposition was performed under a galvanostatic control at a cathodic current density of 40 mA cm^{-2} for 20 min.

Au crystallites were deposited on the ZnCo/Ti surface via the galvanic displacement technique described in Ref. [30]. The prepared ZnCo/Ti catalysts were immersed into the 1 mM $HAuCl_4$ + 0.1 M HCl solution (termed as the Au(III)-containing solution) at 25°C temperature for 0.5, 1 and 5 min, respectively. The surface-to-volume ratio was 1.3 dm^2 l^{-1}. After plating, the samples were taken out, thoroughly rinsed with deionized water and air dried at room temperature. Then, the prepared catalysts were used in alkaline conditions for measurements of the electrochemical oxidation of hydrazine and sodium borohydride without any further treatment.

Characterization of catalysts

The morphology and composition of the fabricated catalysts were characterized using a SEM/FIB workstation Helios Nanolab 650 with an energy dispersive X-ray (EDX) spectrometer INCA Energy 350 X-Max 20.

The Au, Zn and Co metal loadings were estimated from ICP-OES measurements by using an ICP optical emission spectrometer Optima 7000 DV (Perkin Elmer).

Electrochemical measurements

A conventional three-electrode cell was used for electrochemical measurements. The AuZnCo/Ti and ZnCo/Ti catalysts with a geometric area of 2 cm^2 were employed as a working electrode, a Pt sheet was used as a counter electrode and an Ag/AgCl/KCl (3 M KCl) electrode was used as a reference. All electrochemical measurements were performed with a Metrohm Autolab potentiostat (PGSTAT100). Steady state linear sweep voltammograms (CVs) were recorded in 0.05 M N_2H_4 + 1 M NaOH and in 0.05 M $NaBH_4$ + 1 M

NaOH solutions at a linear potential sweep rate of 10 mV s^{-1} at 25°C temperature. The presented current densities were normalized with respect to the geometric area of catalysts. All solutions were deaerated by argon for 30 min prior to measurements.

RESULTS AND DISCUSSION

Material characterization

The morphology and composition of the fabricated catalysts were investigated. Fig. 1b presents the SEM images of the ZnCo/Ti (a) and AuZnCo/Ti catalysts obtained by immersion of the ZnCo/Ti electrode into the Au(III)-containing solution for 0.5 (b), 1 (c) and 5 (d) min. It has been determined that a continuous ZnCo coating with a thickness of ~5 μm was deposited on the titanium surface via the electrochemical deposition technique from the ZnCo plating bath at a cathodic current density of 40 mA cm^{-2} for 20 min. As seen from Fig. 1a, the ZnCo coating fully covers the titanium surface and produces a compact structure with a spherical cluster surface that consists of a large number of smaller nodular-shaped grains ranging from ca. 0.5 μm to ca. 2.5 μm in size. Immersion of the ZnCo/Ti electrodes into the Au(III)-containing solution for various time periods leads to the formation of different size Au nanoparticles on the surface of ZnCo coating (Fig. 1b–d). It is clear that the Au nanoparticles appear in the form of bright cube-shaped crystallites and are homogeneously dispersed on the ZnCo surface. After immersion of the ZnCo/Ti electrode into the Au(III)-containing solution for 0.5 and 1 min, Au crystallites of ca. 16 to 50 nm in size are deposited on the ZnCo/Ti surface (Fig. 1b, c), whereas the immersion of the ZnCo/Ti electrode into the Au(III)-containing solution for 5 min results in the development of somewhat larger Au crystallites onto the ZnCo surface in a range of ca. 50–200 nm in size (Fig. 1d). The samples differ from each other in terms of an average particle size, an interparticle distance and an extent of agglomeration. Although the Au crystallites are hardly discernible in Fig. 1b, c, their residence on the surface of the ZnCo coating is confirmed by the data of EDX analysis. The summarized data are given in Table 1. It shows that the composition of the catalyst stongly depends on the modification time of ZnCo/Ti by Au nanoparticles. The increase in the modification time of the ZnCo coating leads to a higher amount of Au deposited on the surface of the ZnCo/Ti catalyst. In all the cases investigated, a significant amount of Zn and much lower amounts of Au and Co were determined on the surfaces of the mentioned catalysts (Table 1). The loadings of Au in the fabricated AuZnCo/Ti catalysts estimated by the means of ICP-OES measurements are equal to 31, 63 and 306 μg cm^{-2} after the immersion of the ZnCo/Ti electrode into the Au(III)-containing solution for 0.5, 1 and 5 min, respectively.

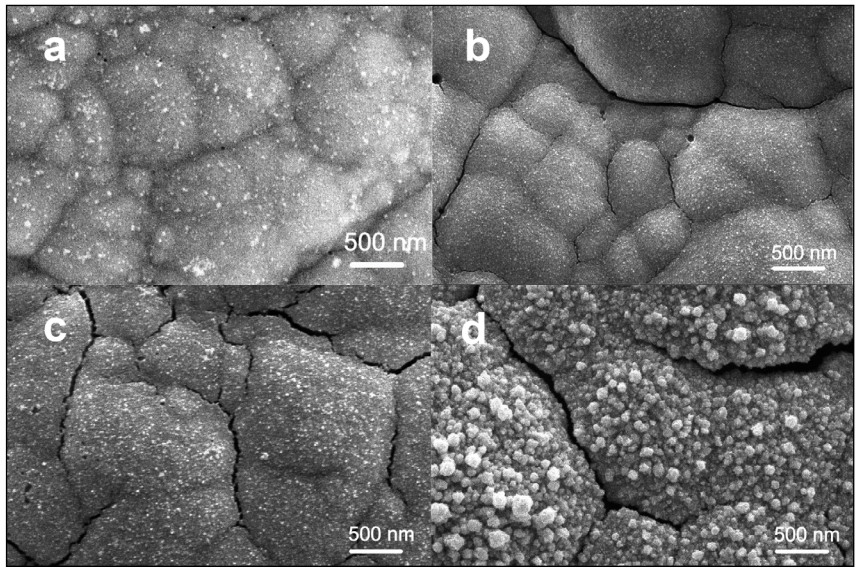

Fig. 1. FESEM images of the as-prepared ZnCo/Ti (a) and AuZnCo/Ti catalysts (b–d). The AuZnCo/Ti catalysts were prepared by ZnCo/Ti immersion into a 1 mM $HAuCl_4$ + 0.1 M HCl solution at 25°C for 0.5 (b), 1 (c) and 5 (d) min

Table 1. **Composition of catalysts determined by ICP-OES and EDX analysis**

Catalyst	Au loading, μg cm^{-2}	Co loading, μg cm^{-2}	Zn loading, μg cm	Element, at.%				
				Au	Zn	Co	O	Ti
ZnCo/Ti	–	827	4550	–	77.92	18.73	3.21	0.15
Au(ZnCo)/Ti	31	875	4470	0.81	74.71	19.27	5.00	0.21
Au(ZnCo)/Ti	63	800	4256	1.49	74.62	19.09	4.54	0.27
Au(ZnCo)/Ti	306	752	2811	11.09	38.29	34.87	15.15	0.60

Electrochemical activity of AuZnCo/Ti catalysts for hydrazine and borohydride oxidation reaction

Electrochemical behaviour of the prepared ZnCo/Ti and AuZnCo/Ti catalysts for HOR and BOR in an alkaline medium was investigated using cyclic voltammetry. Figure 2 shows the typical CVs for the ZnCo/Ti catalyst recorded in the 1 M NaOH solution (a dotted line) and in that containing 0.05 M N_2H_4 (a) and 0.05 M $NaBH_4$ (b) at a potential scan rate of 10 mV s^{-1}. For the ZnCo/Ti electrode well-distinguished anodic peaks (denoted as **A0** and **A**) in a large potential region ranging from –1.2 V to 0.6 V can be observed in the CVs. This indicates that the HOR and BOR are the electrode potential-dependent oxidation process, which proceeds at the latter catalyst. In the case of the supported electrolyte (1 M NaOH), during the anodic scan a well-expressed anodic peak **A0** located at low potential values of ca. –0.9 V is seen in the CVs plots recorded on the ZnCo/Ti (Fig. 2, dotted lines). It should be noted that Zn can be electrochemically oxidized in the alkaline solution at rather negative potential values (as compared to that at the Co/Ti and ZnCo/Ti electrode) by the reaction [57, 58]:

$$2Zn + 4OH^- \Leftrightarrow 2ZnO + 2H_2O + 4e^-$$

$$(E_0 = -1.44 \text{ V vs. Ag/AgCl, pH 14}). \quad (7)$$

Meanwhile, the formation of cobalt oxide and hydroxide could proceed exactly in the same potential region of anodic peak **A0** according to the following reactions [56, 59, 60]:

$$Co + 2OH^- \rightarrow Co(OH)_2 + 2e^-,$$

$$(E_0 = -0.918 \text{ V vs. Ag/AgCl, pH 14}), \quad (8)$$

$$Co + 2OH^- \rightarrow CoO + H_2O + 2e^-$$

$$(E_0 = -0.892 \text{ V vs. Ag/AgCl, pH 14}). \quad (9)$$

In the case of 0.05 M N_2H_4 + 1 M NaOH (Fig. 2a) the magnitude of the current density in the region of the aforementioned peak **A0** remains almost of the same value as compared to that in the background solution of 1 M NaOH (a dotted line). This phenomenon points to the fact that the current densities recorded at low potential values at the ZnCo/Ti electrode in an alkaline hydrazine solution originate essentially from the oxidation of the catalyst surface.

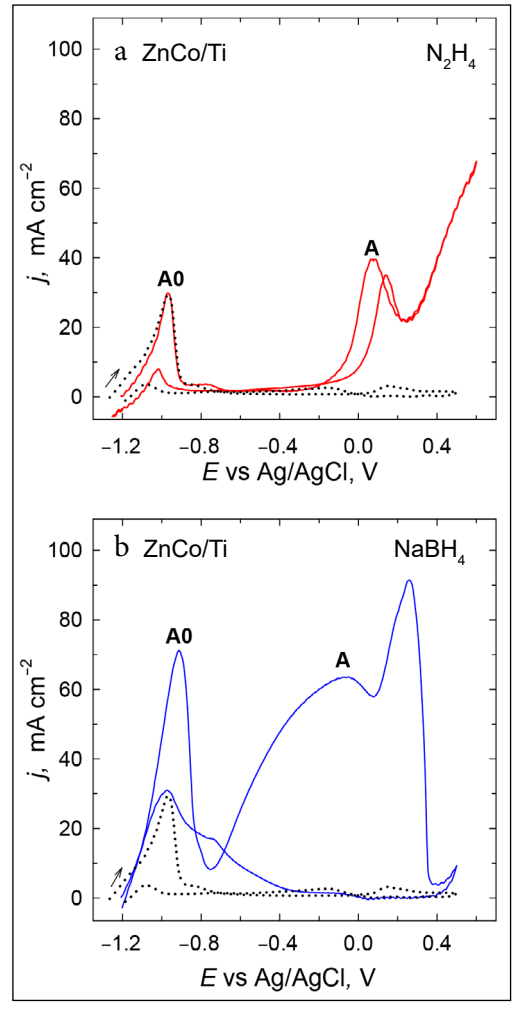

Fig. 2. CVs for the ZnCo/Ti catalyst recorded in 1 M NaOH (dotted lines), 0.05 M N_2H_4 + 1 M NaOH (a), and 0.05 M $NaBH_4$ + 1 M NaOH (b) at a sweep rate of 10 mV s^{-1} at 25°C

However, in the case of the 0.05 M $NaBH_4$ + 1 M NaOH solution (Fig. 2b), the nature of the aforementioned peak **A0** becomes more complicated, since an almost twofold increase in the current density is observed. It is rather plausible that this increase in current additionally involves the oxidation of H_2 generated by the catalytic hydrolysis of sodium borohydride as well as the oxidation of borohydride ions simultaneously. Moreover, at more positive potentials a broad duplet peak **A** for 0.05 M $NaBH_4$ + 1 M NaOH and the same but significantly less wide for 0.05 M N_2H_4 + 1 M NaOH solution emerge (Fig. 2a, b). In those particular cases, higher current density values are measured as compared with the current density values recorded in the background solution. The peak denoted as peak **A** can be attributed to the direct electrooxidation processes of hydrazine or borohydride that take place at the investigated catalyst. It should be emphasized that borohydride oxidation at the ZnCo/Ti electrode starts at more negative potentials and almost twice exceeds in current density as compared to that of hydrazine in the potential region ranging from ca. –0.8 V to –0.1 V. The difference in E_{onset} for borohydride and hydrazine is equal to ca. 0.75 V and points to the fact that from the thermodynamic point of view better operation conditions at the ZnCo/Ti surface are met for borohydride fuel cells.

The electrochemical behaviour of the ZnCo/Ti catalyst modified by small amounts of Au crystallites in a range of 31 μg_{Au} cm^{-2} to 306 μg_{Au} cm^{-2} was investigated in an alkaline medium of 1 M NaOH (Fig. 3) in the absence and in the presence of 0.05 M N_2H_4 or 0.05 M $NaBH_4$ solutions (Fig. 4). Almost no influence is observed in typical CVs in a large potential interval for the AuZnCo/Ti catalyst recorded in 1 M NaOH as compared to that for the ZnCo/Ti catalyst (Fig. 3), except a negligible increase in the current density of the anodic peak **A0** for the catalyst with the Au loading of 306 μg_{Au} cm^{-2}.

Figure 4 presents the first potential cycles of the electrochemical oxidation processes of borohydride and hydrazine at the AuZnCo/Ti catalysts with the Au loadings of 31 μg_{Au} cm^{-2} (a dash-dotted line), 63 μg_{Au} cm^{-2} (a dashed line) and 306 μg_{Au} cm^{-2} (a dash-dot-dotted line) in a 0.05 M $NaBH_4$ + 1 M NaOH (a) or 0.05 M N_2H_4 + 1 M NaOH (b) solution at a sweep rate of 10 mV s^{-1}. For the sake of simplicity, only anodic scans are presented. It was determined that the addition of a small amount of Au crystallites

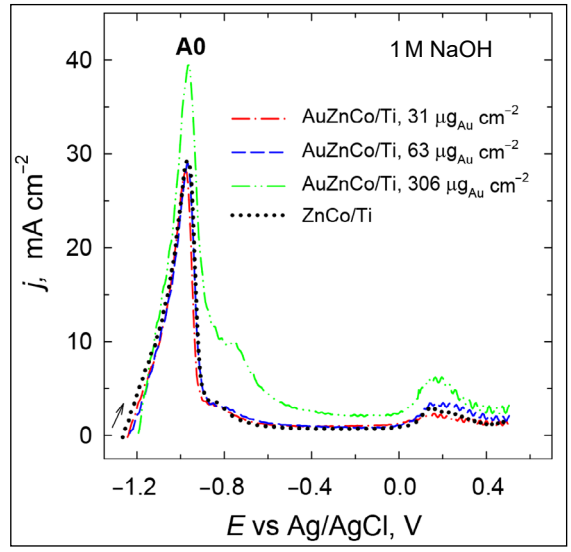

Fig. 3. The positive-going potential scans for the ZnCo/Ti (a dotted line) and AuZnCo/Ti catalysts with the Au loadings of 31 (a dash-dotted line), 63 (a dashed line) and 306 (a dash-dot-dotted line) μg_{Au} cm^{-2} in 1 M NaOH at a sweep rate of 10 mV s^{-1} at 25°C

improves the performance of the ZnCo/Ti catalyst for both borohydride and hydrazine oxidation processes (Fig. 4, dotted lines). CVs plots on the positive-going scan at the AuZnCo/Ti catalysts display a set of well-expressed analogous anodic peaks in almost the same potential regions as in the case of the ZnCo/Ti catalyst. Peak **A0** at lower potential values is followed by a broad one that collapse into a strongly resolved doublet in the case of borohydride solution (Fig. 4a) and less pronounced in the case of hydrazine oxidation (Fig. 4b) (peak **A**). The nature of those peaks could be attributed to the same processes as mentioned above for the ZnCo/Ti catalyst. However, it is clearly seen that the modification of the ZnCo/Ti catalyst with small amounts of Au results both in a potential shift to more negative values under peak **A** and to a significant increase in current density values under the both anodic peaks **A0** and **A** for all the catalysts with Au loadings in a range from of 31 μg_{Au} cm^{-2} to 306 μg_{Au} cm^{-2}. This appropriate feature is especially pronounced for the hydrazine oxidation process (Fig. 4b). It has been determined that the AuZnCo/Ti catalysts with the Au loadings of 31, 63 and 306 μg cm^{-2} show enhanced catalytic activity towards electro-oxidation of hydrazine ions as compared to that of the ZnCo/Ti catalyst. Ca. 1.4–2.3 and 2.0–2.7 times higher hydrazine oxidation current densities under peaks **A0** and **A**, respectively, are at AuZnCo/Ti with the mentioned Au loadings

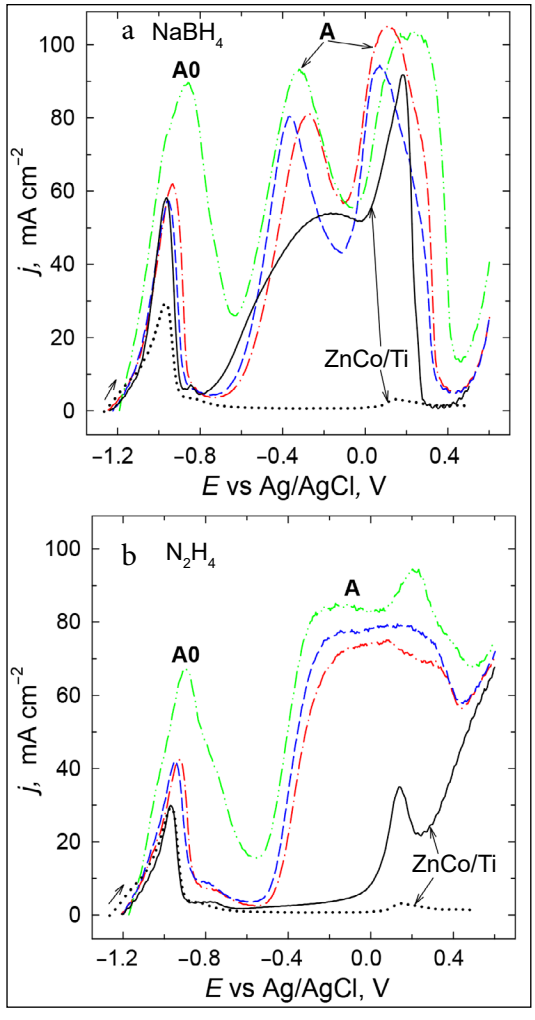

Fig. 4. The first anodic scans for $NaBH_4$ (a) and N_2H_4 (b) oxidation recorded at ZnCo/Ti (a solid line) and AuZnCo/Ti catalysts with the Au loadings of 31 μg_{Au} cm^{-2} (a dash-dotted line), 63 μg_{Au} cm^{-2} (a dashed line) and 306 μg_{Au} cm^{-2} (a dash-dot-dotted) in 0.05 M $NaBH_4$ + 1 M NaOH (a) and in 0.05 M N_2H_4 + 1 M NaOH (b) at a sweep rate of 10 mV s^{-1}; 25°C. The dotted lines represent the anodic scan at ZnCo/Ti recorded in 1 M NaOH

than those at ZnCo/Ti. Similar enhanced catalytic activity towards electrooxidation of borohydride ions at the AuZnCo/Ti catalysts as compared to that of the ZnCo/Ti catalyst was observed in the potential region of peak **A**. Ca. 1.5 times higher anodic current densities were observed at the AuZnCo/Ti catalyst with the Au loading of 31 and 63 μg_{Au} cm^{-2} as compared with that at the ZnCo/Ti catalysts at the abovementioned anodic peak **A**. The current densities measured on the AuZnCo/Ti catalyst with the Au loading of 306 μg_{Au} cm^{-2} are ca. 1.8 times higher than those at the ZnCo/Ti electrode. Interaction of Au nanoparticles with ZnCo leads to higher activities for hydrazine or borohydride oxidation as compared to those at an unmodified ZnCo catalyst. The synergistic effect between the metals present in the catalyst composition promotes the oxidation of hydrazine and borohydride. Meanwhile, this effect is more pronounced for the oxidation of hydrazine on the AuZnCo/Ti catalysts. Moreover, this assumption could be supported by the finding in Ref. [53], where hydrazine oxidation on the Ti catalyst modified by Au nanoparticles was shown to take place at a potential of –0.55 V (vs Ag/AgCl), which was 0.53 V less than polycrystalline Au electrode.

To get thorough information on the influence of the ZnCo/Ti catalyst, modified with small amounts of Au, on hydrazine and borohydride oxidation in a wide potential region applied, which is commonly attributed to the direct electrooxidation processes, the ratio $j_{AuZnCo/Ti}/j_{ZnCo/Ti}$ was calculated and is presented in Fig. 5. In the case of the hydrazine oxidation process, it is clearly visible that this ratio gets the highest value of ca. 28 at the catalyst with the Au loading of 306 μg_{Au} cm^{-2} at a potential value of ca. ~ –0.3 V. Furthermore, this ratio obtained at catalysts with Au loadings of 31 and 63 μg_{Au} cm^{-2} is slightly lower and equals to ca. 20 and 22, respectively. Moreover, the abrupt increase in the ratio $j_{AuZnCo/Ti}/j_{ZnCo/Ti}$ emerges at rather negative potentials in a range of –0.4 V to 0.0 V pointing to the fact that the modification of the ZnCo/Ti catalyst by negligible amounts of Au leads to a tremendous increase in the direct hydrazine oxidation rate and it starts at more negative potentials as compared to that of the unmodified ZnCo/Ti catalyst (Fig. 2a). Meanwhile, in the case of borohydride oxidation, modification of the ZnCo/Ti catalyst with Au crystallites remains significantly less expressed. In this particular case, the ratio $j_{AuZnCo/Ti}/j_{ZnCo/Ti}$ value is only of ca. 1.5–2.2 at E = ~ –0.4 V and shows almost no apparent difference whether the ZnCo/Ti catalyst was modified considerably or not. From the data presented it unambiguously follows that the modification of the ZnCo/Ti catalyst with small amounts of Au has an enormous impact on the process of hydrazine electrooxidation and outperforms that of borohydride, since the calculated ratio $j_{AuZnCo/Ti}/j_{ZnCo/Ti}$ differs in values of ca. 13–18 times at E = ~ –0.4 V.

To compare the activity of the investigated AuZnCo/Ti catalysts the hydrazine and borohydride oxidation current densities for both anodic peaks **A0** and **A** were normalized by the Au loadings

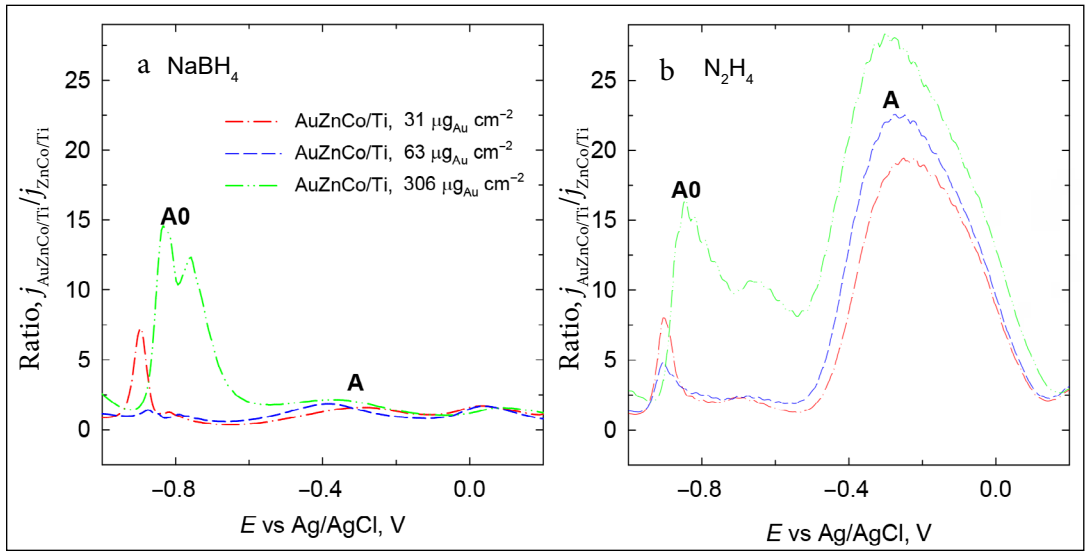

Fig. 5. The ratio of $j_{AuZnCo/Ti}/j_{ZnCo/Ti}$ for N_2H_4 and $NaBH_4$ oxidation calculated from the data in Fig. 4

for each catalyst to represent the mass activity of catalysts. The obtained data are shown in Fig. 6. As evident from Fig. 6 the highest Au mass activity for both hydrazine (a, b) and borohydride (c, d) oxidation processes shows the AuZnCo/Ti catalyst with the lowest Au loading of 31 μg cm^{-2} as compared with that at the AuZnCo/Ti catalyst with Au loadings of 63 and 306 μg cm^{-2}.

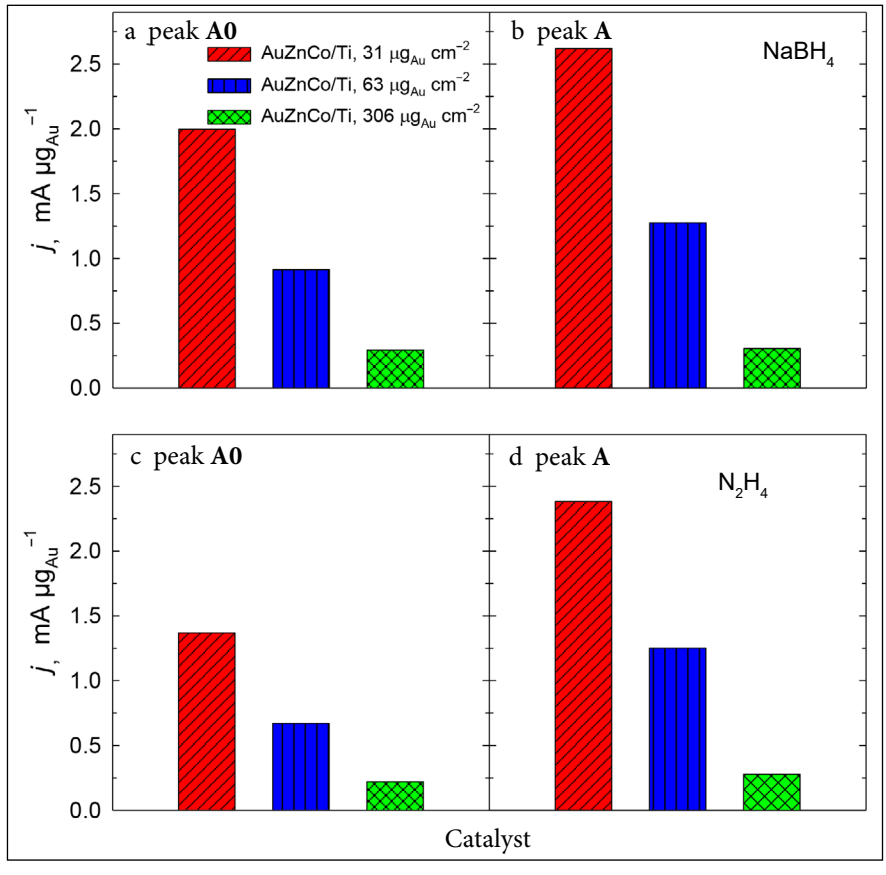

Fig. 6. Bar columns of current densities at peaks **A0** and **A** for the AuZnCo/Ti catalysts with Au loadings of 31, 63 and 306 μg cm^{-2} recorded in 0.05 M N_2H_4 + 1 M NaOH (a–b) and in 0.05 M $NaBH_4$ + 1 M NaOH (c–d) and normalized by the Au loadings for each catalyst

CONCLUSIONS

The activity of the prepared AuZnCo/Ti and ZnCo/Ti catalysts has been examined towards the oxidation of hydrazine and sodium borohydride. Catalysts have been synthesized using the electrochemical deposition technique followed by the simple and low-cost galvanic displacement one. It has been determined that the AuZnCo/Ti catalysts with Au loadings of 31, 63 and 306 μg cm^{-2} show enhanced catalytic activity towards the electrooxidation of both hydrazine and borohydride ions as compared to that of the unmodified ZnCo/Ti catalyst. Ca. 1.4–2.3 and 2.0–2.7 times higher hydrazine oxidation current densities under peaks **A0** and **A**, respectively, are determined at AuZnCo/Ti with different Au loadings than those arising at ZnCo/Ti. Meanwhile, the borohydride oxidation current densities under peak **A** are ca. 1.5–1.8 times higher at AuZnCo/Ti with the same Au loadings than compared to the oxidation current densities at ZnCo/Ti.

It has been found that the interaction of Au nanoparticles with ZnCo leads to higher activities for hydrazine or borohydride oxidation as compared to those at an unmodified ZnCo catalyst.

Received 9 May 2019
Accepted 27 May 2019

References

1. D. M. F. Santos, C. A. C. Sequeira, *Renew. Sustain. Energy Rev*. **15**, 3980 (2011).
2. J. Ma, N. A. Choudhury, Y. Sahai, *Renew. Sustain. Energy Rev.*, **14**, 183 (2010).
3. J.-H. Wee, *J. Power Sources*, **161**, 1 (2006).
4. E. Kjeanga, N. Djilali, D. Sintona, *J. Power Sources*, **186**, 353 (2009).
5. A. Serov, Ch. Kwak, *Appl. Catal., B*, **98**, 1 (2010).
6. T. Sakamoto, A. Serov, T. Masuda, et al., *J. Power Sources*, **375**, 291 (2018).
7. G. L. Soloveichik, *Beilstein J. Nanotech.*, **5**, 1399 (2014).
8. B. H. Liu, Z. P. Li, *J. Power Sources*, **187**, 527 (2009).
9. U. B. Demirci, O. Akdim, J. Andrieux, et al., *Fuel Cells*, **10**, 335 (2010).
10. S. S. Muir, X. Yao, *Int. J. Hydrogen Energy*, **36**, 5983 (2011).
11. S. G. Pakdehi, M. Salimi, M. Rasoolzadeh, *J. Res. Appl. Mech. Eng.* (*RAME*), **3**, 21 (2014).
12. X. Cheng, Z. Shi, N. Glass, et al., *J. Power Sources*, **165**, 739 (2007).
13. M. Petek, S. Bruckenstein, *J. Electroanal. Chem. Interfacial Electrochem*., **47**, 329 (1973).
14. V. Rosca, M. T. M. Koper, *Phys. Chem. Chem. Phys.* **8**, 2513 (2006).
15. M. Chatenet, F. Micoud, I. Roche, E. Chainet, *Electrochim. Acta*, **51**, 5459 (2006).
16. D. M. F. Santos, C. A. C. Sequeira, *Electrochim. Acta*, **55**, 6775 (2010).
17. S. Li, L. Wang, J. Chu, H. Zhu, Y. Liu, *Int. J. Hydrogen Energy*, **41**, 8583 (2016).
18. L. Yi, Y. Song, X. Liu, et al., *Int. J. Hydrogen Energy*, **36**, 15775 (2011).
19. L. Tamašauskaitė-Tamašiūnaitė, A. Jagminienė, A. Balčiūnaitė, et al., *Int. J. Hydrogen Energy*, **38**, 14232 (2013).
20. P. He, X. Wang, P. Fu, H. Wang, L. Yi, *Int. J. Hydrogen Energy*, **36**, 8857 (2011).
21. A. Balčiūnaitė, Z. Sukackienė, L. Tamašauskaitė-Tamašiūnaitė, et al., *Electrochim. Acta*, **225**, 255 (2017).
22. B. Šljukić, J. Milikić, D. M. F. Santos, et al., *Electrochim. Acta*, **107**, 577 (2013).
23. F. Pei, Y. Wang, X. Wang, et al., *Int. J. Hydrogen Energy*, **35**, 8136 (2013).
24. L. Tamašauskaitė-Tamašiūnaitė, A. Balčiūnaitė, A. Zabielaitė, et al., *J. Electroanal. Chem*., **700**, 1 (2013).
25. P. He, Y. Wang, X. Wang, et al., *J. Power Sources*, **196**, 1042 (2011).
26. P. He, X. Wang, Y. Liu, X. Liu, L. Yi, *Int. J. Hydrogen Energy*, **37**, 11984 (2012).
27. S. Papadimitriou, A. Tegou, E. Pavlidou, et al., *Electrochim. Acta*, **53**, 6559 (2008).
28. A. Tegou, S. Papadimitriou, I. Mintsouli, et al., *Catal. Today*, **170**, 126 (2011).
29. M. Abdolmaleki, I. Ahadzadeh, H. Goudarziafshar, *Int. J. Hydrogen Energy*, **42**, 15623 (2017).
30. L. Tamašauskaitė-Tamašiūnaitė, J. Rakauskas, A. Balčiūnaitė, et al., *J. Power Sources*, **72**, 362 (2014).
31. S. S. Narwade, B. B. Mulik, S. M. Mali, et al., *Appl. Surf. Sci.*, **396**, 939 (2017).
32. Y.-C. Shi, T. Yuan, J.-J. Feng, et al., *J. Colloid Interface Sci.*, **505**, 14 (2017).
33. D. C. de Oliveira, W. O. Silva, M. Chatenet, et al., *Appl. Catal., B* **201**, 22 (2017).
34. L. Q. Ye, Z. P. Li, H. Y. Qin, et al., *J. Power Sources*, **196**, 956 (2011).
35. S. J. Lao, H. Y. Qin, L. Q. Ye, et al., *J. Power Sources*, **195**, 4135 (2010).
36. D. M. Yu, Y. Shen, Z. Ye, et al., *Chin. Sci. Bull.*, **58**, 2435 (2013).
37. M. G. Hosseini, M. Abdolmaleki, S. Ashrafpoor, *Chin. J. Catal.*, **33**, 1817 (2012).
38. M. Mitov, G. Hristov, E. Hristova, et al., *Environ. Chem. Lett.*, **7**, 167 (2009).
39. M. G. Hosseini, M. Abdolmaleki, *Int. J. Hydrogen Energy*, **38**, 5449 (2012).

40. M. G. Hosseini, M. Abdolmaleki, F. Nasirpouri, *Electrochim. Acta*, **114**, 215 (2013).
41. K. Asazawa, K. Yamada, H. Tanaka, et al., *Angew. Chem. Int. Ed.*, **119**, 8170 (2007); *Angew. Chem. Int. Ed.*, **46**, 8024 (2007).
42. K. Asazawa, K. Yamada, H. Tanaka, et al., *J. Power Sources*, **191**, 362 (2009).
43. D. A. Geraldo, C. A. Togo, J. Limson, et al., *Electrochim. Acta*, **53**, 8051 (2008).
44. R. Liu, X. Jiang, F. Guo, et al., *Electrochim. Acta*, **94**, 214 (2013).
45. P. Muthukumar, S. A. John, *J. Solid State Electrochem.*, **18**, 2393 (2014).
46. J. Sanabria-Chinchilla, K. Asazawa, T. Sakamoto, et al., *J. Am. Chem. Soc.*, **133**, 5425 (2011).
47. Y. Meng, X. Zou, X. Huang, et al., *Adv. Mater.*, **26**, 6510 (2014).
48. T. Sakamoto, D. Matsumura, K. Asazawa, et al., *Electrochim. Acta*, **163**, 116 (2015).
49. D. A. Finkelstein, R. Imbeaul, S. Garbarino, et al., *J. Phys. Chem*. C, **120**, 4717 (2016).
50. A. Serov, M. Padilla, A. J. Roy, et al., *Angew. Chem.*, **53**, 10336 (2014).
51. U. Martinez, K. Asazawa, B. Halevi, et al., *Phys. Chem. Chem. Phys*., **14**, 5512 (2012).
52. T. Sakamoto, K. Asazawa, J. Sanabria-Chinchilla, et al., *J. Power Sources,* **247**, 605 (2014).
53. M. Jafarian, T. Rostami, M. G. Mahjani, et al., *J. Electroanal. Chem.*, **763**, 134 (2016).
54. L. Tamašauskaitė-Tamašiūnaitė, A. Balčiūnaitė, S. Lichušina, et al., *J. Electrochem. Soc.*, **162**, F348 (2015).
55. S. Lichušina, A. Chodosovskaja, A. Selskis, et al., *Chemija*, **19**, 7 (2008).
56. S. Lichušina, A. Chodosovskaja, K. Leinartas, et al., *J. Solid State Electrochem.*, **14**, 1577 (2010).
57. J. Hong, B. Fang, C. Wang, et al., *J. Power Sources*, **161**, 753 (2006).
58. D. M. F. Santos, C. A. C. Sequeira, *J. Electrochem. Soc*., **157**, B13 (2010).
59. L. D. Burke, M. E. Lyons, O. J. Murphy, *J. Electroanal. Chem.*, **132**, 247 (1982).
60. W. K. Bell, J. E. Toni, *J. Electroanal. Chem.*, **31**, 63 (1971).

Aušrinė Zabielaitė, Aldona Balčiūnaitė, Dijana Šimkūnaitė, Jūratė Vaičiūnienė, Algirdas Selskis, Leonas Naruškevičius, Loreta Tamašauskaitė-Tamašiūnaitė, Eugenijus Norkus

NATRIO BOROHIDRIDO IR HIDRAZINO OKSIDACIJOS TYRIMAS ANT AUKSO NANODALELĖMIS MODIFIKUOTOS CINKO-KOBALTO DANGOS

S a n t r a u k a

Tirta hidrazino ir natrio borohidrido elektrocheminė oksidacija šarminiuose tirpaluose, naudojant modifikuotas Au nanokristalitais ZnCo dangas, nusodintas ant titano paviršiaus (AuZnCo/Ti). AuZnCo/Ti katalizatoriai, turintys skirtingą Au įkrovą, buvo formuojami naudojant elektrocheminį metalų nusodinimo ir galvaninio pakeitimo metodus. Gautų katalizatorių paviršiaus morfologija bei struktūra buvo tirta skenuojančios elektroninės mikroskopijos, rentgeno spindulių energijos dispersinės analizės ir indukuotos plazmos optinės emisijos spektroskopijos metodais. Katalizatorių elektrokatalitinis aktyvumas hidrazino ir natrio borohidrido oksidacijos reakcijai šarminėje terpėje buvo tirtas taikant ciklinę voltamperometriją.

Nustatyta, kad AuZnCo/Ti katalizatoriai, turintys 31, 63 ir 306 μg cm^{-2} Au įkrovą, pasižymi daug stipresniu katalitiniu aktyvumu tiek hidrazino, tiek ir natrio borohidrido oksidacijos reakcijoms, palyginti su nemodifikuotu ZnCo/Ti katalizatoriumi.